ACS Energy LETTERS

http://pubs.acs.org/journal/aelccp

LETTER

Enhanced Fill Factor through Chalcogen Side-Chain Manipulation in Small-Molecule Photovoltaics

Thomas J. Aldrich,[†,§] Matthew J. Leonardi,[†,§] Alexander S. Dudnik,[†,§] Nicholas D. Eastham,[†,§] Boris Harutyunyan,[‡] Thomas J. Fauvell,[†,#] Eric F. Manley,[†,#] Nanjia Zhou,[⊥] Melanie R. Butler,[†] Tobias Harschneck,[†] Mark A. Ratner,[†] Lin X. Chen,[†,#] Michael J. Bedzyk,[‡,⊥] Robert P. H. Chang,[⊥] Ferdinand S. Melkonyan,[*,†] Antonio Facchetti,[*,†,∥] and Tobin J. Marks[*,†,⊥]

[†]Department of Chemistry and the Argonne-Northwestern Solar Energy Research Center, Northwestern University, Evanston, Illinois 60208, United States

[‡]Department of Physics and Astronomy and the Argonne-Northwestern Solar Energy Research Center, Northwestern University, Evanston, Illinois 60208, United States

[⊥]Department of Materials Science and Engineering and the Argonne-Northwestern Solar Energy Research Center, Northwestern University, Evanston, Illinois 60208, United States

[#]Chemical Science and Engineering Division, Argonne National Laboratory, 9700 South Cass Avenue, Lemont, Illinois 60439, United States

[∥]Flexterra Corporation, 8045 Lamon Avenue, Skokie, Illinois 60077, United States

Supporting Information

ABSTRACT: The fill factor (FF) of organic photovoltaic (OPV) devices has proven difficult to optimize by synthetic modification of the active layer materials. In this contribution, a series of small-molecule donors (SMDs) incorporating chalcogen atoms of increasing atomic number (*Z*), namely oxygen, sulfur, and selenium, into the side chains are synthesized and the relationship between the chalcogen *Z* and the FF of OPV devices is characterized. Larger *Z* chalcogen atoms are found to consistently enhance FF in bulk-heterojunction OPVs containing $PC_{61}BM$ as the acceptor material. A significant ∼8% FF increase is obtained on moving from O to S to Se across three series of SMDs. The FF enhancement is found to result from the combination of more ordered morphology and decreased charge recombination in blend films for the high-*Z*-chalcogen SMDs. Because this FF enhancement is found within three series of SMDs, the overall strategy is promising for new SMD materials design.

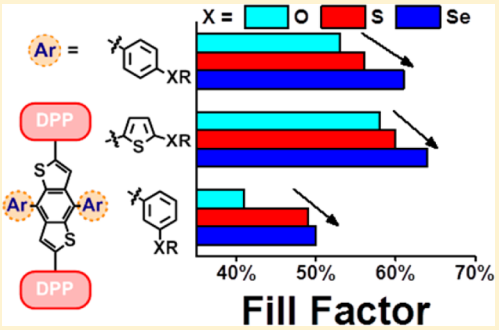

Organic photovoltaic (OPV) materials have garnered considerable attention in recent years as a low-cost renewable energy technology.[1] The basis for this technology is the bulk-heterojunction (BHJ) architecture, which consists of a blend of electron-donating (p-type) and electron-accepting (n-type) organic semiconductors.[2] This blend provides an energetic offset driving photogenerated excitons, bound electron−hole pairs, to separate into free charges, thereby generating electrical current.[3] Among the organic materials used in BHJ blends, small-molecule donors (SMDs) have proven themselves desirable materials capable of achieving high power conversion efficiencies (PCEs).[4−6] Compared to polymer donors, SMDs offer several attractions due to inherent properties such as monodispersity and lack of batch-to-batch molecular weight variation, making them ideal models for studying structure−property relationships in complex BHJ blends.[7,8]

OPV PCEs are calculated from the relationship PCE = J_{SC}·V_{OC}·FF/P_{in}, where J_{SC}·V_{OC}·FF is the output power (P_{out}); P_{in} the power incident on the device; J_{SC} the short-circuit current density; V_{OC} the open-circuit voltage; and FF the fill factor, a parameter related to the ratio of device charge recombination and charge extraction.[9,10] While success has been achieved in optimizing J_{SC} and V_{OC} through molecular structure modifications,[11−15] FF has proven far more challenging to understand and optimize. FF values for OPV SMDs (50−

Received: August 14, 2017
Accepted: September 13, 2017
Published: September 13, 2017

DOI: 10.1021/acsenergylett.7b00743
ACS Energy Lett. 2017, 2, 2415−2421

70%)[16−18] have typically lagged behind those of polymers (up to 80%),[19] so general molecular design strategies to increase FFs would be beneficial in developing new high-performing SMD OPV materials.

Strategies to increase OPV FFs should minimize charge recombination and maximize charge extraction.[9,20] One strategy to enhance charge transport in organic semiconductors is by incorporating large atomic number (Z), polarizable heteroatoms that promote intermolecular interactions.[12,21−23] Specifically, the inclusion of chalcogens in the solubilizing side chains of organic semiconductors typically enhances charge carrier mobility while enabling fine-tuning of frontier molecular orbital (FMO) energy levels; however, the influence on OPV FFs is currently unclear.[21,24−29] Therefore, we sought to enhance FF by systematically introducing chalcogen atoms of increasing Z to improve intermolecular connectivity and create better charge-transporting pathways. To this end, a series of SMDs containing electron-rich benzodithiophene (BDT) and electron-poor diketopyrrolopyrrole (DPP) units connected in an alternating fashion (DPP−BDT−DPP, Figure 1a) were

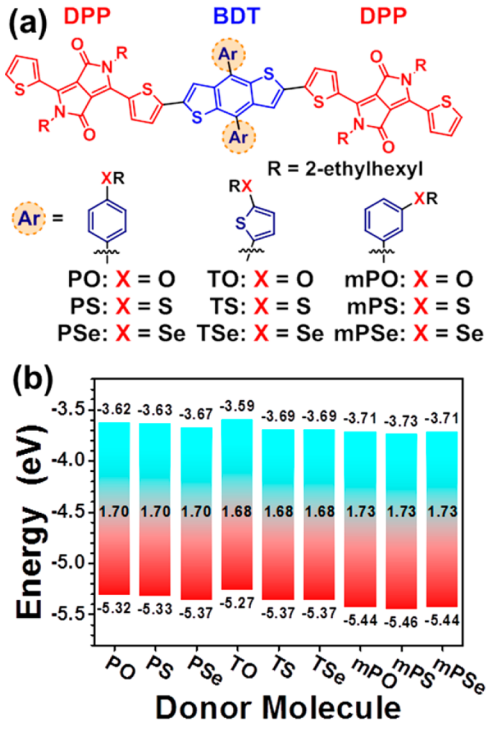

Figure 1. (a) Chemical structures of the PX, TX, and mPX SMDs. (b) Experimental FMO energies and optical band gaps derived from cyclic voltammetry and optical spectroscopy.

synthesized where the functionalization on the central BDT core consists of an aromatic ring connected to a branched alkyl chain via a chalcogen atom, namely oxygen,[21,25,30−32] sulfur,[21,25,31,32] or unprecedented selenium. Three different heteroaromatic units were investigated: *para*-phenyl (**PX**), 2-thienyl (**TX**), and *meta*-phenyl (**mPX**). The DPP−BDT−DPP architecture is known to provide consistent and reproducible SMD PCE values of ∼5%,[8,30,32−37] making this SMD family an excellent candidate for model studies. The present findings show that incorporation of higher Z chalcogen atoms into the SMD side chains generally enhances OPV performance, with larger Z chalcogen atoms consistently yielding higher FFs for all three BDT cores. A detailed study of device blend morphology and charge recombination is performed to understand the origin of the increased FFs.

The SMDs were synthesized by Stille coupling of the appropriate bis(trimethylstannyl) BDT with monobrominated DPP (Scheme S1; see Supporting Information for detailed procedures). The physicochemical properties of the new SMDs were next investigated. The optical band gaps and FMO energies (Figure 1b, Table S2) were obtained by ultraviolet−visible (UV−vis) spectroscopy (Figure S1) and cyclic voltammetry (CV, Figure S2). The optical band gaps of 1.70, 1.68, and 1.73 eV are the same across each aromatic series of **PX**, **TX**, and **mPX**, respectively, with all SMDs exhibiting similar extinction coefficients of $\sim 10^5$ M^{-1} cm^{-1} in solution. Introduction of the next higher Z chalcogen generally lowers the highest occupied molecular orbital (HOMO) energy in the **PX** and **TX** series by 0.05−0.1 eV, while for the **mPX** series the HOMOs remain in a narrow range with **mPS** having the lowest HOMO. The reduction in HOMO energy in the **PX** and **TX** series is caused by a reduction in overlap between the chalcogen atom p-orbitals and the π-orbitals of the SMD as the chalcogen Z increases,[38] while the relatively constant **mPX** HOMO energies are likely a result of the inability of the *meta* chalcogen substituents to π-donate into the SMD backbone. Additionally, the lowest-lying FMOs among these SMDs of ca. −5.45 eV (HOMO) and −3.72 eV (lowest unoccupied molecular orbital, LUMO) are in the **mPX** series. Overall, the variations in electronic structure across these SMDs are small. Density functional theory computed orbital energies (Table S1) agree with the experimental trends of decreasing HOMO energy with increasing chalcogen Z. Melting points (T_m) and enthalpies of fusion (ΔH_{fus}) were determined from differential scanning calorimetry (DSC; Figures S3 and S4, Table S3). T_m and ΔH_{fus} values for the **PX** (308−289 °C, 54.9−47.2 J/g) and **TX** (286−274 °C, 50.1−43.5 J/g) series fall with increasing chalcogen Z, suggesting decreased lattice cohesion, while the opposite trend (218−227 °C, 34.5−46.0 J/g) is found for the **mPX** series.

Next, BHJ OPVs using the SMD series as the donor paired with $PC_{61}BM$ as the acceptor were fabricated and evaluated (details in the Supporting Information). We employed 1,8-diiodooctane (DIO) as a solvent additive for fabrication of all devices as it has been shown to improve device performance for structurally similar SMDs when used in small amounts.[35,39,40] Overall, it is found that the **mPX** SMDs afford PCEs that are markedly lower than those of the **TX** and **PX** series (Table 1). The V_{OC} values trend upward with chalcogen atom Z, tracking the general trend of decreasing SMD HOMO energy (Figure 1b). Values of J_{SC} trend differently depending on the side chain type, with the **TX** series exhibiting a small decrease and the **mPX** series a larger increase from O → S → Se. The **PX** SMDs do not display either trend, with the greatest J_{SC} achieved by **PS**, followed by **PO** and **PSe** (Figure 2). Importantly, the FF increases by a relative 6−8% with increasing chalcogen atom Z *in all three SMD series*. While this FF increase does not afford a higher PCE in all cases because of the variations in J_{SC} discussed earlier, the result is striking given the consistency of the trend. To investigate the origin of this FF modulation, we focused on characterizing the **PX** series.

The **PX** series blend film morphology was first investigated by transmission electron microscopy (TEM) to understand how the chalcogen affects the donor−acceptor phase segregation (Figure 3). **PO** blends exhibit large but ill-defined regions of SMD and $PC_{61}BM$ in the 100+ nm size. In contrast,

DOI: 10.1021/acsenergylett.7b00743
ACS Energy Lett. 2017, 2, 2415−2421

Table 1. SMD OPV Device Parameters

SMD[a]	PCE (%)	V_{oc} (V)	J_{sc} (mA cm^{-2})	FF (%)
PO[c]	3.66 ± 0.02	0.792 ± 0.002	8.76 ± 0.13	52.7 ± 0.3
PS[b]	4.92 ± 0.08	0.817 ± 0.006	10.81 ± 0.17	55.7 ± 0.8
PSe[c]	3.73 ± 0.09	0.872 ± 0.015	7.05 ± 0.02	60.7 ± 0.6
TO[c]	3.83 ± 0.08	0.720 ± 0.014	9.18 ± 0.05	57.96 ± 0.15
TS[b]	4.40 ± 0.02	0.804 ± 0.002	9.07 ± 0.15	60.32 ± 0.18
TSe[b]	4.54 ± 0.07	0.786 ± 0.008	8.94 ± 0.05	64.5 ± 0.3
mPO[c]	0.60 ± 0.06	0.633 ± 0.022	2.39 ± 0.13	41.2 ± 0.7
mPS[c]	0.96 ± 0.03	0.815 ± 0.002	2.40 ± 0.04	48.7 ± 0.4
mPSe[c]	1.60 ± 0.07	0.821 ± 0.008	4.01 ± 0.14	49.86 ± 0.02

[a]1:1 w:w% blend with $PC_{61}BM$ spin-cast from 1% v/v DIO in $CHCl_3$. [b]Calculated from the values for 10 devices. [c]Calculated from the values for 8 devices.

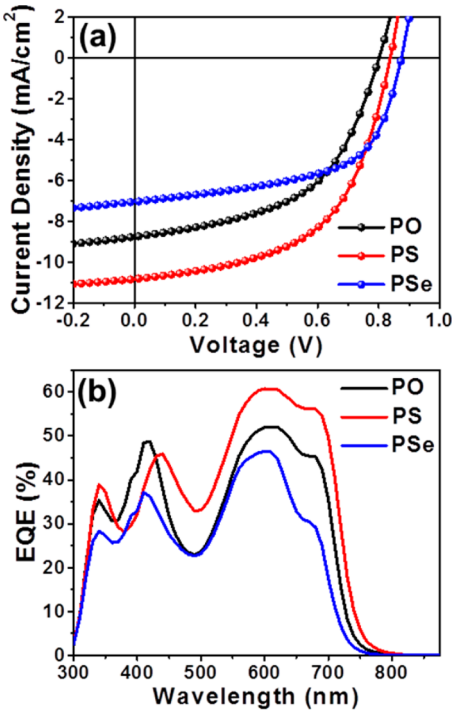

Figure 2. (a) *J*–*V* and (b) EQE characteristics of PO-, PS-, and PSe-based OPV devices.

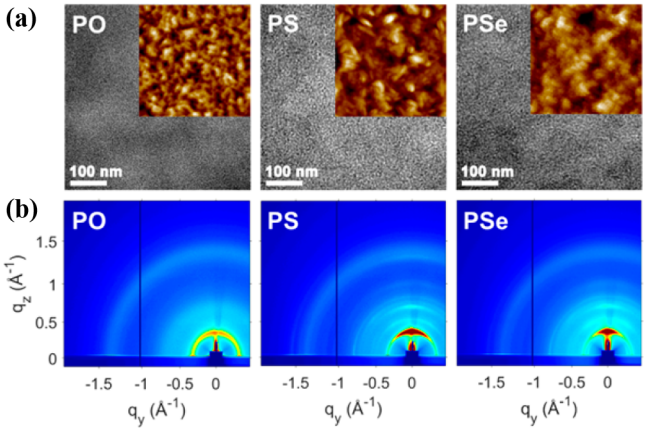

Figure 3. Images of SMD:$PC_{61}BM$ blend films: (a) TEM and AFM (insets, 2 μm × 2μm) and (b) 2D GIWAXS patterns.

PS blends exhibit a finely interpenetrated network, with much smaller donor and acceptor domain sizes, while **PSe** exhibits a morphology similar to that of **PS**, but the regions of donor and acceptor are more clearly defined. Atomic force microscopy (AFM) images (inset of Figure 3a) of the **PO** blend film exhibit a relatively smooth and amorphous surface versus those of **PS** and **PSe**. **PS** exhibits the roughest blend film surface with needle-like crystalline features. The corresponding RMS roughness values of **PO**, **PS**, and **PSe** films are 3.60, 18.4, and 8.26 nm, respectively. This suggests formation of more crystalline films for **PS** and **PSe** blends compared to those of **PO**. Grazing incidence wide-angle X-ray scattering (GIWAXS; Figure 3b) analysis of the blends shows that all three **PX** SMDs are predominantly oriented "edge-on" with respect to the substrate, with decreasing amounts of "face-on" character on moving from **PSe** to **PO** to **PS**. Lamellar *d*-spacings of 18.0 Å (in-plane) and 18.4 Å (out-of-plane) were found for **PS** and **PSe**, while larger values of 19.0 Å (in-plane) and 18.9 Å (out-of-plane) are found for **PO**, suggesting a tighter lamellar packing for SMDs with larger *Z* heteroatoms. The $\pi-\pi$ stacking region shows a very weak reflection for **PO** with a *d*-spacing of 3.93 Å both in-plane and out-of-plane. In contrast, **PS** and **PSe** exhibit only in-plane peaks which are far more intense and have *d*-spacings of 4.07 and 4.08 Å, respectively. Interestingly, this trend is exactly opposite to the *d*-spacing contraction seen in some chalcogen-containing polymer systems.[29] Scherrer analysis of the crystalline domain size shows that **PO** exhibits small lamellar crystallites of 9.9 nm in-plane and 7.0 nm out-of-plane, while **PS** and **PSe** exhibit larger lamellar crystallites of 13.2 nm (in-plane) and 14.0 nm (out-of-plane) for **PS**, and 12.2 nm (in-plane) and 11.8 nm (out-of-plane) for **PSe**, confirming the AFM results. Importantly, $\pi-\pi$ crystallite sizes are greater for the higher *Z* chalcogens, with values of 20.9 nm and 20.2 nm for **PS** and **PSe**, respectively, while **PO** is much smaller at 4.2 nm in-plane and 3.9 nm out-of-plane. Overall, these results suggest that while O incorporation leads to tighter $\pi-\pi$ stacking due to the smaller size of the heteroatom, S and Se promote greater crystalline order in thin films.

We next sought to analyze the charge recombination behavior of the **PX** SMDs to examine the effect of chalcogen variation. The two types of charge recombination in OPVs are monomolecular geminate recombination, in which an exciton recombines before separating into free carriers, and non-geminate recombination, where separated carriers encounter an opposite charge that is free (bimolecular) or trapped (monomolecular), both of which lower the FF.[41] To investigate

DOI: 10.1021/acsenergylett.7b00743
ACS Energy Lett. 2017, 2, 2415–2421

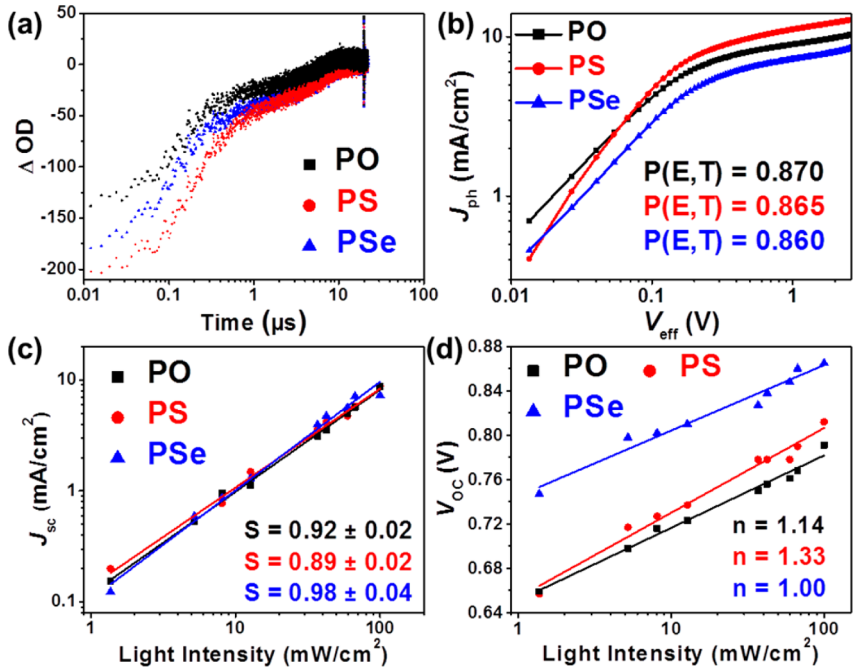

Figure 4. (a) Decay plots for nsTA of PX blend films. (b) Log–log plots of J_{ph} vs V_{eff} and (c) J_{SC} vs I for OPV devices. (d) Semilog plot of V_{OC} vs I.

the rates and mechanisms of nongeminate recombination on **PX** series blend films, nanosecond transient absorption (nsTA) spectroscopy was employed. The films were excited at 650 nm, and the ground-state bleach between 680 and 700 nm was monitored. This long-lived bleach signal (on the order of microseconds) is attributed to free charge carriers.[42,43] Typical nsTA decay curves for OPV blend films exhibit two distinct decay components: one fast (<20 ns) and one slow (300 ns to 10 μs).[44] The fast decay component, which has been shown to be extremely dependent on charge carrier concentration and laser pump fluence, is typically attributed to recombination of free, mobile charge carriers. In contrast, the slow decay component is typically attributed to recombination from carriers bound in trap sites. The slow decay component shows two unique characteristics: a pump fluence dependent magnitude that saturates at higher fluence and a fluence-independent power law dependence on time $\Delta OD \propto t^{-\alpha}$.[42,44,45] Note that, at intensities around 1 sun illumination, recombination kinetics are likely determined by this slow recombination mechanism.[46] Decay curves shown in Figure 4a exhibit the recovery of the ground-state bleach in the three blends. Considering the slow decay component (starting at 1 μs and moving to longer times), there is a clear difference in behavior between **PO** and the other blends. When fitting to a power law, **PO** returns an α value of 0.61, while **PS** and **PSe** both return α values of 0.26, indicating overall faster recombination in the **PO** blend. These stark differences indicate a fundamental difference between **PO** and the other two blends, which is consistent with the observed decreased order and smaller crystalline domain sizes, resulting in more trap-based recombination.[47] However, this does not account for the difference in FF between **PS** and **PSe**, suggesting the presence of additional factors.

To understand the extent of geminate recombination in the present OPVs, the photocurrent, J_{ph} ($J_{ph} = J_L - J_D$, where J_L is the current under illumination and J_D is the dark current) was measured as a function of the effective voltage, V_{eff}, ($V_{eff} = V_0 - V_a$, where V_0 is the voltage at which $J_{ph} = 0$, and V_a is the applied bias) and plotted on a log–log scale (Figure 4b).[48] Then, the exciton dissociation probability $P(E,T)$, defined as the ratio of J_{ph}/J_{sat} at J_{SC} where J_{sat} is the saturation current at high effective voltage,[49] was calculated. We find $P(E,T)$ values of 0.870, 0.865, and 0.860 for **PO**, **PS**, and **PSe**, respectively. The similar values of $P(E,T)$ for the SMDs suggest there is little difference in the exciton dissociation properties and imply that the major recombination pathway is nongeminate.

Light intensity (I) dependent J–V analysis of the OPVs was next performed to understand the influence of bimolecular recombination and space-charge effects. The relationship between J_{SC} and I is defined as $J_{SC} \propto I^S$, where the S value gives information about the efficiency of bimolecular recombination.[50,51] Deviation from $S = 1$ indicates losses due to space-charge build-up or substantial bimolecular recombination, which will be the only recombination mechanisms operating at such high internal fields in an OPV device.[50] Interestingly, S values are found to be 0.92, 0.89, and 0.98 for **PO**, **PS**, and **PSe**, respectively. These results indicate weak bimolecular recombination in the **PSe** blend and more efficient recombination in **PO** and **PS** blends (Figure 4c). The role of charge transport in the blend was also studied by measuring the space-charge limited current (SCLC) mobilities of single carrier diodes fabricated by sandwiching a blend film between contacts that promote either hole or electron injection (details in the Supporting Information). The results show that **PSe** has a hole mobility (μ_h) greater than those of **PO** and **PS** (Table 2),

Table 2. SCLC Charge Carrier Mobilities and Thicknesses of PX:$PC_{61}BM$ Blend Films

SMD	μ_h ($\times 10^{-6}$ cm^2 V^{-1} s^{-1})	μ_e ($\times 10^{-6}$ cm^2 V^{-1} s^{-1})	film thickness (nm)
PO	1.8 ± 0.3	13 ± 6	84 ± 1.2
PS	1.3 ± 0.2	30 ± 4	83 ± 1.5
PSe	4.4 ± 0.3	4.4 ± 0.4	86 ± 1.6

DOI: 10.1021/acsenergylett.7b00743
ACS Energy Lett. 2017, 2, 2415–2421

which are not substantially different. Electron mobilities (μ_e) are greater for **PO** and **PS** than for **PSe**. The similar μ_h values for the **PO** and **PS** blends can be attributed to a balance between the larger degree of "face-on" orientation in **PO** and higher crystallinity in **PS**, both of which known to correlate with increased μ_h.[20,52−54] Likewise, the largest μ_h found for **PSe** is in agreement with the high degree of crystallinity and increased "face-on" orientation. As charge extraction in OPVs has been shown to be predominantly influenced by the mobility of the slower charge carrier,[55,56] the highest μ_h for **PSe** implies that holes will be extracted most easily from this device. The lower μ_h values of the **PO** and **PS** blends imply that hole extraction is a more difficult process. Considering the charge recombination dynamics seen in the nsTA, the slower decay of the **PS** blend allows more time for charges to be extracted before recombination than in the **PO** blend.[57] This trend also implies that recombination pathways involving triplet states appear not to be enhanced in this SMD series by the ability of large Z atoms such as S or Se to promote intersystem crossing.[58] These findings suggest a decreased contribution from nongeminate recombination with increasing chalcogen Z.

To elucidate the contribution of other recombination processes, the relationship between V_{OC} and I was investigated. This dependence is governed by the relation $V_{OC} = n(k_BT/e)\ln(I) + C$, where n is the ideality constant, k_b the Boltzmann constant, T temperature, e elementary charge, and C a constant.[50,59] A value of $n = 1$ indicates that bimolecular recombination is the only recombination mechanism, while $n > 1$ indicates both bimolecular and monomolecular recombination are occurring.[50] The values of n in the **PO**, **PS**, and **PSe** blends were found to be 1.14, 1.33, and 1.00, respectively (Figure 4d). It can be concluded that bimolecular recombination is the only recombination process occurring in the **PSe** blend, while **PO** and **PS** devices exhibit both bimolecular and monomolecular recombination.[50] Clearly, the slow nsTA decay kinetics, a high μ_h, and the absence of monomolecular recombination lead to the highest FF in the **PSe** devices.

In conclusion, a series of SMDs containing chalcogen-functionalized aromatic side-chain substituents was synthesized, and their OPV performance was characterized. Increasing the Z of the chalcogen atom significantly enhances the FF in these devices. SMDs containing large Z chalcogens exhibit increased crystalline order and reduced charge recombination, both of which contribute to their higher FF values. Importantly, this FF increase is not limited to a specific aromatic moiety on the BDT core, but this effect is evident across three separate SMD series. This finding lays the groundwork for a general design rule for organic solar cells with high FFs.

■ ASSOCIATED CONTENT

Supporting Information

The Supporting Information is available free of charge on the ACS Publications website at DOI: 10.1021/acsenergylett.7b00743.

Synthetic and experimental details, ^{1}H NMR spectra, UV−vis absorption spectra, CV traces, DSC curves, J-V curves for SCLC diodes, and GIWAXS linecuts (PDF)

■ AUTHOR INFORMATION

Corresponding Authors

*E-mail: f-melkonyan@northwestern.edu.
*E-mail: a-facchetti@northwestern.edu.
*E-mail: t-marks@northwestern.edu.

ORCID

Alexander S. Dudnik: 0000-0001-9014-7660
Michael J. Bedzyk: 0000-0002-1026-4558
Ferdinand S. Melkonyan: 0000-0001-8228-9247
Tobin J. Marks: 0000-0001-8771-0141

Author Contributions

§T.J.A., M.J.L., A.S.D., and N.D.E. contributed equally to the experimental work.

Notes

The authors declare no competing financial interest.

■ ACKNOWLEDGMENTS

This research was supported in part by the Argonne-Northwestern Solar Energy Research (ANSER) Center, an Energy Frontier Research Center funded by the U.S. Department of Energy, Office of Science, Office of Basic Energy Sciences under Award Number DE-SC0001059 (N.Z., T.J.F., B.H.) and by AFOSR Grant FA9550-15-1-0044 (A.F. materials design). Use of the Advanced Photon Source, an Office of Science User Facility operated for the U.S. Department of Energy (DOE) Office of Science by Argonne National Laboratory, was supported by the U.S. DOE under Contract No. DE-AC02-06CH11357. This work made use of the EPIC, Keck-II, and/or SPID facilities of Northwestern University's NUANCE Center, which has received support from the Soft and Hybrid Nanotechnology Experimental (SHyNE) Resource (NSF ECCS-1542205); the MRSEC program (NSF DMR-1121262) at the Materials Research Center; the International Institute for Nanotechnology (IIN); the Keck Foundation; and the State of Illinois, through the IIN. A.S.D. thanks the Camille and Henry Dreyfus Postdoctoral Program in Environmental chemistry for a fellowship; T.J.A. and M.R.B. thank the NSF for predoctoral fellowships; M.J.L. thanks the ASEE for an NDSEG fellowship; and T.H. thanks the DAAD for a postdoctoral fellowship. F.S.M. was supported by Award 70NANB14H012 from U.S. Department of Commerce, National Institute of Standards and Technology as part of the Center for Hierarchical Materials Design (CHiMaD), and E.F.M. was supported by Qatar NPRP Grant 7-286-1-049.

■ REFERENCES

(1) Lu, L.; Zheng, T.; Wu, Q.; Schneider, A. M.; Zhao, D.; Yu, L. Recent Advances in Bulk Heterojunction Polymer Solar Cells. *Chem. Rev.* **2015**, *115*, 12666−12731.

(2) Heeger, A. J. 25th Anniversary Article: Bulk Heterojunction Solar Cells: Understanding the Mechanism of Operation. *Adv. Mater.* **2014**, *26*, 10−27.

(3) Clarke, T. M.; Durrant, J. R. Charge Photogeneration in Organic Solar Cells. *Chem. Rev.* **2010**, *110*, 6736−6767.

(4) Deng, D.; Zhang, Y.; Zhang, J.; Wang, Z.; Zhu, L.; Fang, J.; Xia, B.; Wang, Z.; Lu, K.; Ma, W.; et al. Fluorination-Enabled Optimal Morphology Leads to over 11% Efficiency for Inverted Small-Molecule Organic Solar Cells. *Nat. Commun.* **2016**, *7*, 13740.

(5) Ni, W.; Wan, X.; Li, M.; Wang, Y.; Chen, Y. A-D-A Small Molecules for Solution-Processed Organic Photovoltaic Cells. *Chem. Commun.* **2015**, *51*, 4936−4950.

(6) Collins, S. D.; Ran, N. A.; Heiber, M. C.; Nguyen, T. Q. Small Is Powerful: Recent Progress in Solution-Processed Small Molecule Solar Cells. *Adv. Energy Mater.* **2017**, *7*, 1602242.

DOI: 10.1021/acsenergylett.7b00743
ACS Energy Lett. 2017, 2, 2415−2421

(7) Roncali, J.; Leriche, P.; Blanchard, P. Molecular Materials for Organic Photovoltaics: Small Is Beautiful. *Adv. Mater.* **2014**, *26*, 3821−3838.
(8) Tang, A.; Zhan, C.; Yao, J.; Zhou, E. Design of Diketopyrrolopyrrole (DPP)-Based Small Molecules for Organic-Solar-Cell Applications. *Adv. Mater.* **2017**, *29*, 1600013.
(9) Bartesaghi, D.; Perez Idel, C.; Kniepert, J.; Roland, S.; Turbiez, M.; Neher, D.; Koster, L. J. Competition between Recombination and Extraction of Free Charges Determines the Fill Factor of Organic Solar Cells. *Nat. Commun.* **2015**, *6*, 7083.
(10) Mazzio, K. A.; Luscombe, C. K. The Future of Organic Photovoltaics. *Chem. Soc. Rev.* **2015**, *44*, 78−90.
(11) Eastham, N. D.; Dudnik, A. S.; Aldrich, T. J.; Manley, E. F.; Fauvell, T. J.; Hartnett, P. E.; Wasielewski, M. R.; Chen, L. X.; Melkonyan, F. S.; Facchetti, A.; et al. Small Molecule Acceptor and Polymer Donor Crystallinity and Aggregation Effects on Microstructure Templating: Understanding Photovoltaic Response in Fullerene-Free Solar Cells. *Chem. Mater.* **2017**, *29*, 4432−4444.
(12) Ashraf, R. S.; Meager, I.; Nikolka, M.; Kirkus, M.; Planells, M.; Schroeder, B. C.; Holliday, S.; Hurhangee, M.; Nielsen, C. B.; Sirringhaus, H.; et al. Chalcogenophene Comonomer Comparison in Small Band Gap Diketopyrrolopyrrole-Based Conjugated Polymers for High-Performing Field-Effect Transistors and Organic Solar Cells. *J. Am. Chem. Soc.* **2015**, *137*, 1314−1321.
(13) Min, J.; Luponosov, Y. N.; Gerl, A.; Polinskaya, M. S.; Peregudova, S. M.; Dmitryakov, P. V.; Bakirov, A. V.; Shcherbina, M. A.; Chvalun, S. N.; Grigorian, S.; et al. Alkyl Chain Engineering of Solution-Processable Star-Shaped Molecules for High-Performance Organic Solar Cells. *Adv. Energy Mater.* **2014**, *4*, 1301234.
(14) Liang, Y.; Xu, Z.; Xia, J.; Tsai, S. T.; Wu, Y.; Li, G.; Ray, C.; Yu, L. For the Bright Future-Bulk Heterojunction Polymer Solar Cells with Power Conversion Efficiency of 7.4%. *Adv. Mater.* **2010**, *22*, E135−138.
(15) Lai, T.-H.; Constantinou, I.; Grand, C. M.; Klump, E. D.; Baek, S.; Hsu, H.-Y.; Tsang, S.-W.; Schanze, K. S.; Reynolds, J. R.; So, F. Evidence of Molecular Structure Dependent Charge Transfer between Isoindigo-Based Polymers and Fullerene. *Chem. Mater.* **2016**, *28*, 2433−2440.
(16) Li, M.; Liu, F.; Wan, X.; Ni, W.; Kan, B.; Feng, H.; Zhang, Q.; Yang, X.; Wang, Y.; Zhang, Y.; et al. Subtle Balance between Length Scale of Phase Separation and Domain Purification in Small-Molecule Bulk-Heterojunction Blends under Solvent Vapor Treatment. *Adv. Mater.* **2015**, *27*, 6296−6302.
(17) Love, J. A.; Nagao, I.; Huang, Y.; Kuik, M.; Gupta, V.; Takacs, C. J.; Coughlin, J. E.; Qi, L.; van der Poll, T. S.; Kramer, E. J.; et al. Silaindacenodithiophene-Based Molecular Donor: Morphological Features and Use in the Fabrication of Compositionally Tolerant, High-Efficiency Bulk Heterojunction Solar Cells. *J. Am. Chem. Soc.* **2014**, *136*, 3597−3606.
(18) Luponosov, Y. N.; Min, J.; Solodukhin, A. N.; Bakirov, A. V.; Dmitryakov, P. V.; Shcherbina, M. A.; Peregudova, S. M.; Cherkaev, G. V.; Chvalun, S. N.; Brabec, C. J.; et al. Star-Shaped D−π−A Oligothiophenes with a Tris(2-methoxyphenyl)amine Core and Alkyldicyanovinyl Groups: Synthesis and Physical and Photovoltaic Properties. *J. Mater. Chem. C* **2016**, *4*, 7061−7076.
(19) Guo, X.; Zhou, N.; Lou, S. J.; Smith, J.; Tice, D. B.; Hennek, J. W.; Ortiz, R. P.; Navarrete, J. T. L.; Li, S.; Strzalka, J.; et al. Polymer Solar Cells with Enhanced Fill Factors. *Nat. Photonics* **2013**, *7*, 825−833.
(20) Min, J.; Luponosov, Y. N.; Gasparini, N.; Richter, M.; Bakirov, A. V.; Shcherbina, M. A.; Chvalun, S. N.; Grodd, L.; Grigorian, S.; Ameri, T.; et al. Effects of Alkyl Terminal Chains on Morphology, Charge Generation, Transport, and Recombination Mechanisms in Solution-Processed Small Molecule Bulk Heterojunction Solar Cells. *Adv. Energy Mater.* **2015**, *5*, 1500386.
(21) Min, J.; Cui, C. H.; Heumueller, T.; Fladischer, S.; Cheng, X.; Spiecker, E.; Li, Y. F.; Brabec, C. J. Side-Chain Engineering for Enhancing the Properties of Small Molecule Solar Cells: A Trade-Off Beyond Efficiency. *Adv. Energy Mater.* **2016**, *6*, 1600515.
(22) Nakano, M.; Niimi, K.; Miyazaki, E.; Osaka, I.; Takimiya, K. Isomerically Pure Anthra[2,3-*b*:6,7-*b*′]-bifuran (Anti-ADF), -Dithiophene (Anti-ADT), and -Diselenophene (Anti-ADS): Selective Synthesis, Electronic Structures, and Application to Organic Field-Effect Transistors. *J. Org. Chem.* **2012**, *77*, 8099−8111.
(23) Amb, C. M.; Chen, S.; Graham, K. R.; Subbiah, J.; Small, C. E.; So, F.; Reynolds, J. R. Dithienogermole as a Fused Electron Donor in Bulk Heterojunction Solar Cells. *J. Am. Chem. Soc.* **2011**, *133*, 10062−10065.
(24) Kan, B.; Zhang, Q.; Li, M.; Wan, X.; Ni, W.; Long, G.; Wang, Y.; Yang, X.; Feng, H.; Chen, Y. Solution-Processed Organic Solar Cells Based on Dialkylthiol-Substituted Benzodithiophene Unit with Efficiency near 10%. *J. Am. Chem. Soc.* **2014**, *136*, 15529−15532.
(25) Zhou, Z. C.; Xu, S. J.; Liu, W. R.; Zhang, C.; Hu, Q.; Liu, F.; Russell, T. P.; Zhu, X. Z. Applying the Heteroatom Effect of Chalcogen for High-Performance Small-Molecule Solar Cells. *J. Mater. Chem. A* **2017**, *5*, 3425−3433.
(26) Min, J.; Bronnbauer, C.; Zhang, Z.-G.; Cui, C.; Luponosov, Y. N.; Ata, I.; Schweizer, P.; Przybilla, T.; Guo, F.; Ameri, T.; et al. Fully Solution-Processed Small Molecule Semitransparent Solar Cells: Optimization of Transparent Cathode Architecture and Four Absorbing Layers. *Adv. Funct. Mater.* **2016**, *26*, 4543−4550.
(27) Cui, C.; Wong, W.-Y.; Li, Y. Improvement of Open-Circuit Voltage and Photovoltaic Properties of 2D-Conjugated Polymers by Alkylthio Substitution. *Energy Environ. Sci.* **2014**, *7*, 2276−2284.
(28) Jiang, J.-M.; Raghunath, P.; Lin, Y.-C.; Lin, H.-K.; Ko, C.-L.; Su, Y.-W.; Lin, M. C.; Wei, K.-H. Linear Solubilizing Side Chain Substituents Enhance the Photovoltaic Properties of Two-Dimensional Conjugated Benzodithiophene-Based Polymers. *Polymer* **2015**, *79*, 262−270.
(29) Cui, C.; He, Z.; Wu, Y.; Cheng, X.; Wu, H.; Li, Y.; Cao, Y.; Wong, W.-Y. High-Performance Polymer Solar Cells Based on a 2D-Conjugated Polymer with an Alkylthio Side-Chain. *Energy Environ. Sci.* **2016**, *9*, 885−891.
(30) Du, Z.; Chen, W.; Wen, S.; Qiao, S.; Liu, Q.; Ouyang, D.; Wang, N.; Bao, X.; Yang, R. New Benzo[1,2-*b*:4,5-*b*′]dithiophene-Based Small Molecules Containing Alkoxyphenyl Side Chains for High Efficiency Solution-Processed Organic Solar Cells. *ChemSusChem* **2014**, *7*, 3319−3327.
(31) Cui, C.; Wong, W. Y. Effects of Alkylthio and Alkoxy Side Chains in Polymer Donor Materials for Organic Solar Cells. *Macromol. Rapid Commun.* **2016**, *37*, 287−302.
(32) Yao, H.; Ye, L.; Zhang, H.; Li, S.; Zhang, S.; Hou, J. Molecular Design of Benzodithiophene-Based Organic Photovoltaic Materials. *Chem. Rev.* **2016**, *116*, 7397−7457.
(33) Loser, S.; Bruns, C. J.; Miyauchi, H.; Ortiz, R. P.; Facchetti, A.; Stupp, S. I.; Marks, T. J. A Naphthodithiophene-Diketopyrrolopyrrole Donor Molecule for Efficient Solution-Processed Solar Cells. *J. Am. Chem. Soc.* **2011**, *133*, 8142−8145.
(34) Loser, S.; Lou, S. J.; Savoie, B. M.; Bruns, C. J.; Timalsina, A.; Leonardi, M. J.; Smith, J. N.; Harschneck, T.; Turrisi, R.; Zhou, N.; et al. Systematic Evaluation of Structure-Property Relationships in Heteroacene - Diketopyrrolopyrrole Molecular Donors for Organic Solar Cells. *J. Mater. Chem. A* **2017**, *5*, 9217−9232.
(35) Huang, J.; Zhan, C.; Zhang, X.; Zhao, Y.; Lu, Z.; Jia, H.; Jiang, B.; Ye, J.; Zhang, S.; Tang, A.; et al. Solution-Processed DPP-Based Small Molecule That Gives High Photovoltaic Efficiency with Judicious Device Optimization. *ACS Appl. Mater. Interfaces* **2013**, *5*, 2033−2039.
(36) Lin, Y.; Ma, L.; Li, Y.; Liu, Y.; Zhu, D.; Zhan, X. A Solution-Processable Small Molecule Based on Benzodithiophene and Diketopyrrolopyrrole for High-Performance Organic Solar Cells. *Adv. Energy Mater.* **2013**, *3*, 1166−1170.
(37) Eastham, N. D.; Dudnik, A. S.; Harutyunyan, B.; Aldrich, T. J.; Leonardi, M. J.; Manley, E. F.; Butler, M. R.; Harschneck, T.; Ratner, M. A.; Chen, L. X.; et al. Enhanced Light Absorption in Fluorinated Ternary Small-Molecule Photovoltaics. *ACS Energy Lett.* **2017**, *2*, 1690−1697.

DOI: 10.1021/acsenergylett.7b00743
ACS Energy Lett. 2017, 2, 2415−2421

(38) Lee, D.; Stone, S. W.; Ferraris, J. P. A Novel Dialkylthio Benzo[1,2-*b*:4,5-*b*′]dithiophene Derivative for High Open-Circuit Voltage in Polymer Solar Cells. *Chem. Commun.* **2011**, *47*, 10987−10989.
(39) Harschneck, T.; Zhou, N.; Manley, E. F.; Lou, S. J.; Yu, X.; Butler, M. R.; Timalsina, A.; Turrisi, R.; Ratner, M. A.; Chen, L. X.; et al. Substantial Photovoltaic Response and Morphology Tuning in Benzo[1,2-*b*:6,5-*b*′]dithiophene (bBDT) Molecular Donors. *Chem. Commun.* **2014**, *50*, 4099−4101.
(40) Huang, J.; Wang, X.; Zhang, X.; Niu, Z.; Lu, Z.; Jiang, B.; Sun, Y.; Zhan, C.; Yao, J. Additive-Assisted Control over Phase-Separated Nanostructures by Manipulating Alkylthienyl Position at Donor Backbone for Solution-Processed, Non-Fullerene, All-Small-Molecule Solar Cells. *ACS Appl. Mater. Interfaces* **2014**, *6*, 3853−3862.
(41) Proctor, C. M.; Kuik, M.; Nguyen, T.-Q. Charge Carrier Recombination in Organic Solar Cells. *Prog. Polym. Sci.* **2013**, *38*, 1941−1960.
(42) Katoh, R.; Matsuzaki, H.; Furube, A.; Sonar, P.; Williams, E. L.; Vijila, C.; Subramanian, G. S.; Gorelik, S.; Hobley, J. Charge Generation and Recombination in Diketopyrrolopyrrole Polymer: Fullerene Bulk Heterojunctions Studied by Transient Absorption and Time-Resolved Microwave Conductivity. *J. Phys. Chem. C* **2016**, *120*, 28398−28406.
(43) Ohkita, H.; Ito, S. Transient Absorption Spectroscopy of Polymer-Based Thin-Film Solar Cells. *Polymer* **2011**, *52*, 4397−4417.
(44) Nelson, J. Diffusion-Limited Recombination in Polymer-Fullerene Blends and Its Influence on Photocurrent Collection. *Phys. Rev. B: Condens. Matter Mater. Phys.* **2003**, *67*, 155209.
(45) Nogueira, A. F.; Montanari, I.; Nelson, J.; Durrant, J. R.; Winder, C.; Sariciftci, N. S.; Brabec, C. Charge Recombination in Conjugated Polymer/Fullerene Blended Films Studied by Transient Absorption Spectroscopy. *J. Phys. Chem. B* **2003**, *107*, 1567−1573.
(46) Montanari, I.; Nogueira, A. F.; Nelson, J.; Durrant, J. R.; Winder, C.; Loi, M. A.; Sariciftci, N. S.; Brabec, C. Transient Optical Studies of Charge Recombination Dynamics in a Polymer/Fullerene Composite at Room Temperature. *Appl. Phys. Lett.* **2002**, *81*, 3001−3003.
(47) Min, J.; Jiao, X. C.; Ata, I.; Osvet, A.; Ameri, T.; Bauerle, P.; Ade, H.; Brabec, C. J. Time-Dependent Morphology Evolution of Solution-Processed Small Molecule Solar Cells During Solvent Vapor Annealing. *Adv. Energy Mater.* **2016**, *6*, 1502579.
(48) Mihailetchi, V. D.; Wildeman, J.; Blom, P. W. Space-Charge Limited Photocurrent. *Phys. Rev. Lett.* **2005**, *94*, 126602.
(49) Lu, L.; Chen, W.; Xu, T.; Yu, L. High-Performance Ternary Blend Polymer Solar Cells Involving Both Energy Transfer and Hole Relay Processes. *Nat. Commun.* **2015**, *6*, 7327.
(50) Cowan, S. R.; Roy, A.; Heeger, A. J. Recombination in Polymer-Fullerene Bulk Heterojunction Solar Cells. *Phys. Rev. B: Condens. Matter Mater. Phys.* **2010**, *82*, 245207.
(51) Proctor, C. M.; Kim, C.; Neher, D.; Nguyen, T.-Q. Nongeminate Recombination and Charge Transport Limitations in Diketopyrrolopyrrole-Based Solution-Processed Small Molecule Solar Cells. *Adv. Funct. Mater.* **2013**, *23*, 3584−3594.
(52) Guo, J.; Liang, Y.; Szarko, J.; Lee, B.; Son, H. J.; Rolczynski, B. S.; Yu, L.; Chen, L. X. Structure, Dynamics, and Power Conversion Efficiency Correlations in a New Low Bandgap Polymer: PCBM Solar Cell. *J. Phys. Chem. B* **2010**, *114*, 742−748.
(53) Vohra, V.; Kawashima, K.; Kakara, T.; Koganezawa, T.; Osaka, I.; Takimiya, K.; Murata, H. Efficient Inverted Polymer Solar Cells Employing Favourable Molecular Orientation. *Nat. Photonics* **2015**, *9*, 403−408.
(54) Long, G.; Wu, B.; Solanki, A.; Yang, X.; Kan, B.; Liu, X.; Wu, D.; Xu, Z.; Wu, W.-R.; Jeng, U. S.; et al. New Insights into the Correlation between Morphology, Excited State Dynamics, and Device Performance of Small Molecule Organic Solar Cells. *Adv. Energy Mater.* **2016**, *6*, 1600961.
(55) Stolterfoht, M.; Armin, A.; Philippa, B.; White, R. D.; Burn, P. L.; Meredith, P.; Juska, G.; Pivrikas, A. Photocarrier Drift Distance in Organic Solar Cells and Photodetectors. *Sci. Rep.* **2015**, *5*, 9949.
(56) Kaienburg, P.; Rau, U.; Kirchartz, T. Extracting Information About the Electronic Quality of Organic Solar-Cell Absorbers from Fill Factor and Thickness. *Phys. Rev. Appl.* **2016**, *6*, 024001.
(57) Collado-Fregoso, E.; Boufflet, P.; Fei, Z.; Gann, E.; Ashraf, S.; Li, Z.; McNeill, C. R.; Durrant, J. R.; Heeney, M. Increased Exciton Dipole Moment Translates into Charge-Transfer Excitons in Thiophene-Fluorinated Low-Bandgap Polymers for Organic Photovoltaic Applications. *Chem. Mater.* **2015**, *27*, 7934−7944.
(58) Rao, A.; Chow, P. C.; Gelinas, S.; Schlenker, C. W.; Li, C. Z.; Yip, H. L.; Jen, A. K.; Ginger, D. S.; Friend, R. H. The Role of Spin in the Kinetic Control of Recombination in Organic Photovoltaics. *Nature* **2013**, *500*, 435−439.
(59) Koster, L. J. A.; Mihailetchi, V. D.; Ramaker, R.; Blom, P. W. M. Light Intensity Dependence of Open-Circuit Voltage of Polymer:-Fullerene Solar Cells. *Appl. Phys. Lett.* **2005**, *86*, 123509.

DOI: 10.1021/acsenergylett.7b00743
ACS Energy Lett. 2017, 2, 2415−2421